ACS OMEGA

http://pubs.acs.org/journal/acsodf

Article

Investigation of Structural, Mechanical, Optoelectronic, and Thermoelectric Properties of $BaXF_3$ (X = Co, Ir) Fluoro-Perovskites: Promising Materials for Optoelectronic and Thermoelectric Applications

Shaukat Ali Khattak,* Mohammed Abohashrh, Imtiaz Ahmad, Mudasser Husain, Irfan Ullah, Syed Zulfiqar, Gul Rooh, Nasir Rahman, Gulzar Khan, Tahirzeb Khan, Muhammad Salman Khan, Said Karim Shah, and Vineet Tirth

Cite This: *ACS Omega* 2023, 8, 5274−5284

Read Online

ACCESS | Metrics & More | Article Recommendations

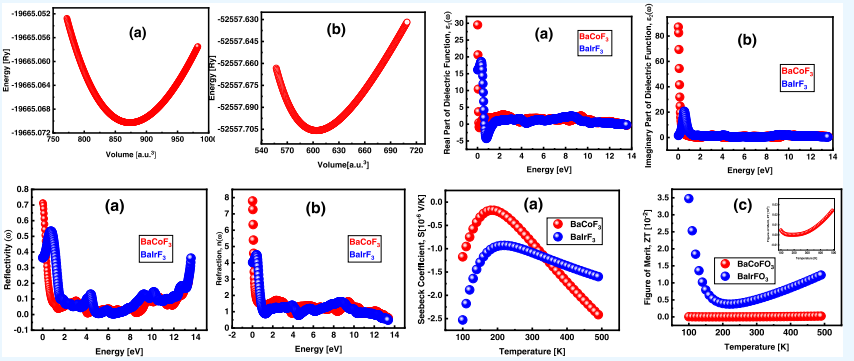

ABSTRACT: Coded within Wien2K, we carry out DFT-based calculations for investigations of the structural, elastic, optoelectronic, and thermoelectric properties of $BaXF_3$ (X = Co, Ir) fluoro-perovskites. The Birch−Murnaghan fit to the energy-vs-volume data and formation energy shows that these fluoro-perovskites are structurally stable. The phonon calculation confirms the thermodynamic stability, while the relation between elastic constants such as $C_{11} - C_{12} > 0$, $C_{11} > 0$, $C_{11} + 2C_{12} > 0$, and $B > 0$ validates the mechanical stability of the compounds. $BaIrF_3$ exhibits a strong ability to endure compressive and shear stresses. $BaCoF_3$ shows a weaker capacity of withstanding changes in volume, attributed to a lower bulk modulus. Demonstrating a higher *G*-modulus of rigidity than the $BaIrF_3$, $BaCoF_3$ demonstrates stronger resistance to change the shape and both compounds are found to be anisotropic and brittle. The determined band structure profiles reveal that both $BaCoF_3$ and $BaIrF_3$ demonstrate a metallic nature. In addition, the metallic nature of $BaCoF_3$ and $BaIrF_3$ is reinforced by the density-of-states (DOS) study, where Co and F atoms contribute significantly to the total DOS in the valence band in the case of $BaCoF_3$, while that of $BaIrF_3$ is predominated by the Ba and F atoms. The computed values of $\varepsilon_1(0)$ for $BaCoF_3$ and $BaIrF_3$ are approximately 30 and 19, respectively, which are in line with Penn's model. The researched materials are confirmed to be strong contenders for optoelectronics by the lack of absorption in the visible range. For their potential use in thermoelectric device applications, thermoelectric parameters such as temperature-dependent Seebeck coefficient, specific heat capacity, thermal conductivity, power factor, and figure of merit are also investigated, which show that these materials are thermally stable and promising for applications in thermoelectric devices.

1. INTRODUCTION

The new interest in cubic fluoro-perovskites (AXF_3), where A and B are cations, is thanks to their promising crystal structure and significant physical characteristics. DFT investigation of different AXF_3 for the determination of their band structure has been performed by Nishimatsu et al.[1] utilizing the local density approximation (LDA) and pseudopotential approach.[2] The research on the use of the solid solution $LiBaCaSrF_3$ on $LiSrF_3$ to produce light-emitting diodes was conducted by the authors, where they inferred their potential use in the development of lenses in the optical lithography steppers.[3]

Received: September 8, 2022
Accepted: January 18, 2023
Published: February 1, 2023

Tran and Blaha's modified Becke and Johnson exchange potential was exploited to study the optoelectronic characteristics of $SrTiO_3$ and $BaTiO_3$ at an ambient temperature while reporting results that are significantly better than those of prior first-principles studies in terms of experimental values.[4] Khan et al. studied the rare earth telluride compounds, Ba_2MYTe_5 (M = Ga, In), where their band gaps were found to be in the range of 1.08−1.36 eV and studied the thermoelectric properties of these compounds.[5] CaS was investigated where the full-potential Green's function multiple-scattering, FLAPW, and finite-difference techniques provided similar Ca and S K-edge spectra.[6] To determine which is wide and direct and optical qualities to forecast their use in the optoelectronic industry, the bonding nature, as well as the structural, electronic, chemical bonding, and optical characteristics of $KCaF_3$, $RbCaF_3$, and $CsCaF_3$, has been explored.[7] The optical characteristics of many systems containing rare earth were investigated, utilizing FP-LAPW GGA and GGA + U approximations.[8−11] However, it was discovered that the developed modified Becke−Johnson potential (TB-mBJ) approximation is more suitable for systems without correlated electrons, primarily semiconductors and insulators. It was better from a computational cost perspective as well as in terms of the outcomes. To describe a drop in bulk modulus and the increase in lattice parameter, Murtaza et al.[12] calculated the electrical and optical characteristics using the TB-mBJ approach. For use in the deep ultraviolet area, solid solutions of $LiKBaMgF_3$ on $LiBaF_3$ were produced.[13] Experimental work on the structural phase transition in $RbCdF_3$ has been done by Studzinski et al.[14] Investigations into the cubic fluoro-perovskites, $ACaF_3$ (where A = K, Rb, Cs), as promising candidates for core-valence luminescence (CVL), have been conducted.[15] The following three factors are critical for CVL: (1) electron energy difference between the core p-states of K, Rb, and Cs and the p-states of F constituting the top of the valence band; (2) the breadth of the upper valence band; and (3) the band gap. Exploiting the ab initio approach, these investigations further rekindled interest in these systems. Cubic perovskites have been studied with a focus on their optical characteristics utilizing the full-potential linearized augmented plane wave (FP-LAPW) approach, using the generalized gradient approximation (GGA) and LDA by Babu et al.,[16] Mousa et al.,[17] and Li et al.[18] To imply an order−disorder nature of the 193 and 50 K phase transitions, researchers analyzed the temperature dependency of structural parameters and phase transition of $RbCaF_3$.[19] However, neither the optical and electrical nor the thermoelectric characteristics of the cubic perovskites $BaXF_3$ (X = Co, Ir) have been previously studied or determined using the TB-mBJ-based approach.[20]

This triggered the conduction of this study while employing the DFT-based FP-LAPW method because mBJ-based calculations are anticipated to produce significant optical qualities that would more precisely address band gaps and transitions. To get insight into these structures, we have therefore investigated their thermoelectric in addition to the optoelectronic properties.

2. COMPUTATIONAL DETAILS AND CRYSTAL STRUCTURE

As depicted in Figure 1, the $BaXF_3$ (X = Co, Ir) compounds with the $Pm\bar{3}m$ space group crystallize in a cubic form. According to the Wyckoff coordinates, the Ba, X (Co and Ir), and fluorine are located at locations **1a** (0, 0, 0), **1b** (0.5, 0.5, 0.5), and **3c** (0, 0.5, 0.5), respectively.[21] A well-known quantum mechanical solution to the many-body issue is DFT.[22] An effective technique to calculate the ground-state characteristics of materials, i.e., the DFT-based FP-LAPW approach encoded in the Wien2k code,[23] was used in this work to perform the first-principles total energy calculations.[24,25] The unit cell was partitioned into (I) interstitial space and (II) nonoverlapping atomic spheres (centered at the atomic sites).

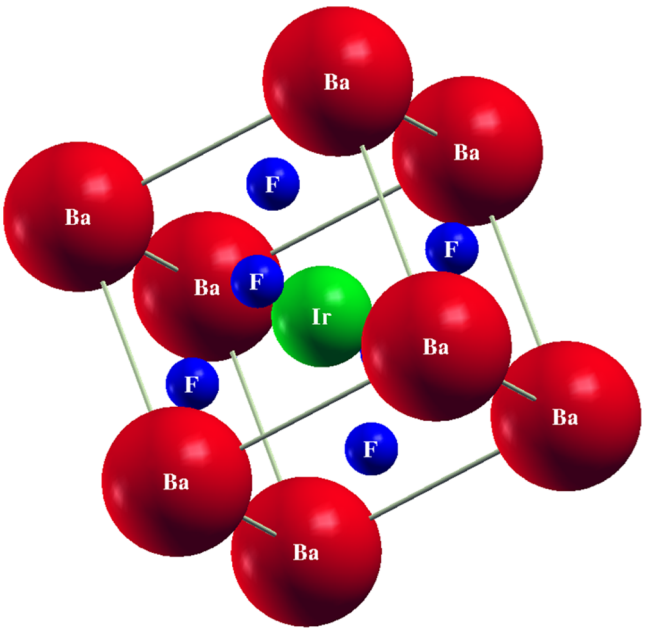

Figure 1. Crystal structure of the $BaIrF_3$ fluoro-perovskite. The $BaCoF_3$ has a similar structure where Ir in this figure is replaced with Co.

Different basis sets are employed in these two different types of areas. The Ba, Co, and F atoms' muffin tin (MT) radii have been set at 2.39, 1.48, and 1.89 a.u., respectively, in $BaCoF_3$. Additionally, in the case of $BaIrF_3$, the MT radii of the Ba, Ir, and F atoms are at 2.49, 1.69, and 1.79 a.u., respectively. Taking 1000 spatial *k*-points in the irreducible wedge of the Brillouin zone (BZ), integrations in the reciprocal space were carried out. The size of the basis sets made up of the plane waves is controlled by the convergence parameters, which are assumed to have a value of $R_{MT} \times K_{MAX} = 8$. For consistency, G_{MAX} is set to 11 $(\text{a.u.})^{-1}$, and convergence is accomplished with a 10^{-3} Ry energy tolerance. The ideal value of the lattice parameters is used to calculate the ground-state electronic structures of the present compound. We evaluated the total energies for the various volumes, which range from −10 to +10% of the experimental (theoretical) lattice parameters to determine the lattice parameters' optimum value.[26,27] Plots of the calculated findings are made using equations given in ref 28.

The most notable achievements employing the mBJ results for semiconductors were the improved band-gap results[29] and the optical characteristic computations in the current FP-LAPW study using the mBJ-based approximation. The electron−hole interaction was considered using the random-phase approximation, although local field effects were not considered.[30,31] Additionally, the BoltzTrap code was used to calculate the thermoelectric (TE) properties.[32] The thermoelectric properties are calculated while exploiting the Onsager relations and the Boltzmann transport theory.

https://doi.org/10.1021/acsomega.2c05845
ACS Omega 2023, 8, 5274−5284

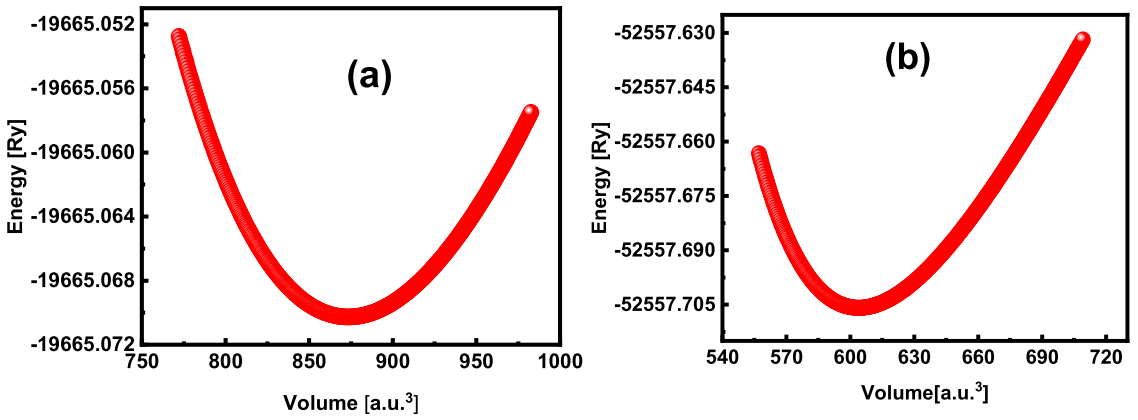

Figure 2. Optimized energy vs. volume for (a) $BaCoF_3$ and (b) $BaIrF_3$ fluoro-perovskites.

3. RESULTS AND DISCUSSION

3.1. Structural and Mechanical Properties. Figure 2 displays the Birch−Murnaghan-fitted optimum energy curves for the cubic $BaCoF_3$ and $BaIrF_3$ fluoro-perovskites employing the TB-mBJ technique. The ground-state energy (E_0), ground-state volume (V_0), the structure's bulk modulus (B_0), and pressure derivative (B_0') are all predicted by these computations. The parameters associated with the point are considered the ground-state energy and volume.[33−36] The materials' ground state is found by looking into the points in the curve where the lowest energy relative to the volume is fitted with the Birch−Murnaghan equation. The ground-state volume can be utilized to calculate lattice constants. In addition to the volume optimization by the Birch−Murnaghan equation of state, the thermodynamic stability was checked by determining the formation energy (H_f) for both compounds by using eq 1

$$H_f = E_{BaXF_3} - (aE_{Ba} + bE_X + cE_F) \quad (1)$$

where E_{BaXF_3} and E_{Ba}, E_X, and E_F are the total energy of the compound and energy of Ba, X (Co, Ir), and F, respectively. The a, b, and c represent the number of Ba, X (Co, Ir), and F, respectively. The calculated formation energies for $BaCoF_3$ and $BaIrF_3$ are −1.48 and −19 438.68 Ry, respectively. The negative formation energies of the compounds suggest that they are thermodynamically stable where the $BaIrF_3$ exhibits more thermodynamic stability than the $BaCoF_3$.

Table 1 provides a summary of the structural parameters of $BaCoF_3$ and $BaIrF_3$ fluoro-perovskites.

The thermodynamic stability was determined by carrying out the phonon calculation, as shown in Figure 3, which exhibits no imaginary frequencies, and the only frequencies are those that are real for both $BaCoF_3$ and $BaIrF_3$. This suggests that both compounds demonstrate thermodynamic stability.

Table 1. Structural Parameters Such As Lattice Parameter (a_0), Bulk Modulus (B_0), Pressure Derivative (B_0'), Ground-State Energy (E_0), and Formation Energy (H_f) of the BXF_3 (X = Co, Ir) Fluoro-Perovskites

structural parameter	$BaCoF_3$	$BaIrF_3$
a_0 (Å)	4.21	4.54
V_0 (a.u^3)	503.74	608.09
B_0 (GPa)	79.79	149.90
B_0'	4.03	108.46
E_0 (Ry)	−19 665.07	−52 557.70
H_f (Ry)	−1.48	−1.17

Furthermore, the mechanical stability of the compounds was analyzed by calculating and characterizing their elastic properties by determining the elastic constants as they demonstrate the materials' response to the applied forces, i.e., reveal the mechanical characteristics of materials. Therefore, these constants provide information about the mechanical stability and toughness of the materials. The components of the stress tensor for tiny strains were computed at zero pressure, and the energy was put per the lattice strain, which maintained the volume constant.[37] The IRelast package, built specifically for cubic systems and interfaced with WIEN2K, was used to calculate the elastic constants. There are only three independent elastic constants C_{ij} in total for cubic structures, namely, C_{11}, C_{12}, and C. Various elastic parameters, of the materials, given in Table 2, were determined by using equations given in the work carried out by Khattak et al.[38]

The elastic constants must be related to each other for the cubic crystal mechanical stability: $C_{11} - C_{12} > 0$, $C_{11} > 0$, $C_{11} + 2C_{12} > 0$, and $B > 0$.[39] According to Table 2, which shows that the researched materials comply with these requirements, they are inferred to be mechanically stable. $BaIrF_3$ has greater elastic stiffness coefficients, which shows that the material has a strong ability to endure compressive as well as shear stresses, according to Table 2. $BaCoF_3$, on the other hand, has a lower bulk modulus, which indicates a weaker capacity to withstand changes in volume. Additionally, the fact that $BaCoF_3$ has a higher G-modulus of rigidity than $BaIrF_3$ suggests that it has a stronger ability to resist shape change. According to the values of A, no compound is entirely isotropic. It is interesting to note that the materials' B/G ratio is negative, which suggests the brittle nature of both compounds.[40]

3.2. Electronic Band Structure and Density of States. Electronic properties establish the role of materials in their technological uses and are also responsible for determining many of their physical properties, particularly thermoelectric transport properties. The approaches for computing electronic characteristics were largely introduced in the past decades owing to the DFT and improvements in programming knowledge and computing capacity. Numerous DFT-based computational algorithms may be used to properly calculate the electronic structure of materials. Scf computations have been used to analyze the electronic characteristics of materials.[41−43] The two main factors that influence how the

https://doi.org/10.1021/acsomega.2c05845
ACS Omega 2023, 8, 5274−5284

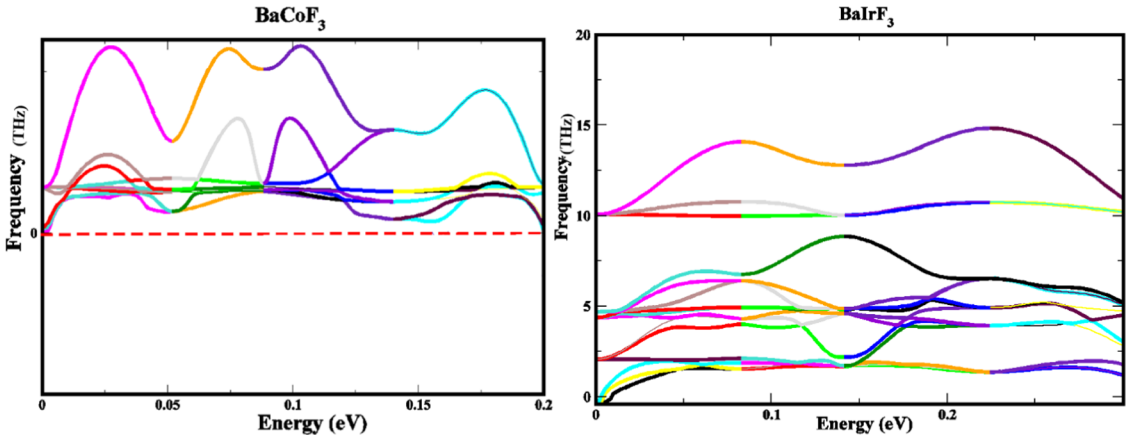

Figure 3. Frequency vs. energy while using phonon calculations for $BaCoF_3$ and $BaIrF_3$.

Table 2. Elastic Parameters for $BaCoF_3$ and $BaIrF_3$: Elastic Stiffness Coefficients (C_{11}, C_{12}, and C_{44}), Bulk Modulus (B), and Zener's Constant (A)[a]

elastic parameters	$BaCoF_3$	$BaIrF_3$
C_{11} (GPa)	57.4	84.7
C_{12} (GPa)	45.7	50.0
C_{44} (GPa)	−11.3	−22.9
B (GPa)	47.9	60.7
A	−1.9	−1.3
G_v (GPa)	−4.4	−6.8
G_R (GPa)	−8.1	−35.2
G (GPa)	−6.3	−21.0
E (GPa)	−19.6	−71.1
V	0.9	1.1
B/G	−7.9	−2.9

[a] G_v, G_R, and G are the Voigt shear modulus, Reuss shear modulus, and mean of G_v and G_R, respectively. E is the elastic modulus, V is Poisson's ratio, and B/G is the ratio of bulk to shear moduli. The elastic stiffness coefficients and other constants as well as pressure are in GPa and volume in $bohr^3$.

materials' electronic properties are determined are the band structure and DOS. With the aid of the modified Becke−Johnson (mBJ) potential and the unit cell's optimized design, the electronic characteristics of the materials were calculated together with a high symmetric point of the Brillouin zone. Figure 4 shows calculated electronic band structures of the examined compounds $BaCoF_3$ [Figure 4a] and $BaIrF_3$ [Figure 4b], fluoro-perovskites, which show that the minima of conduction and maxima of valence bands overlap with each other around the Fermi level. This implies that both $BaCoF_3$ and $BaIrF_3$ exhibit metallic behavior.

We further estimated the DOS, which are shown in Figures 5 and 6, to get insight into the electrical characteristics of the present structures. The results of band structures are corroborated by the total density of states (TDOS) of $BaCoF_3$ [Figure 5] and $BaIrF_3$ [Figure 6] fluoro-perovskites, which further confirms their metallic nature. In the case of $BaCoF_3$ [Figure 5a], the TDOS is predominantly contributed by fluorine in the energy range lying in the valence band [between −10 and −6 eV] and around the Fermi level in the valence band cobalt dominates the contribution to the total density of states. In the conduction-band energy region, the density of states is mainly contributed by the barium. Figure 5b exhibits the total density of states for the $BaCoF_3$ and the contribution of the partial density of states (PDOS) toward it, where the TDOS is mainly contributed by the F-p PDOS in the valence band between −9.5 and −6.5 eV, while the Co-d PDOS has the contribution near the Fermi level in the valence band. In the conduction band, the TDOS is mainly caused by the Ba-d PDOS. The contribution of all PDOS in both valence and conduction bands is overshadowed.

Figure 6a shows that the TDOS of $BaIrF_3$ is caused majorly by the F atom in the valence band, which is maximum at −2.0 eV, while in the conduction band the Ba atom mainly contributes to the TDOS at 4.0 eV while at the other energy of the conduction band, the TDOS is lesser while fluctuating from one energy to another.

The presence of the DOS around the Fermi level also reinforces the revelation of Figure 4b, i.e., the $BaIrF_3$ exhibits a metallic behavior, which is attributed to the PDOS of Ir and F atoms as evident from Figure 6b, where the PDOS are populated around the Fermi level. In the valence band, the F-d has the highest contribution, while it is overshadowed by the Ba-d in the conduction band. All other PDOS are hard to be noticed. This also shows that Ba-d and F-d orbitals contribute in a mixed manner to the development of the CB of $BaIrF_3$.

3.3. Optical Properties. Exploring the emission of $BaCoF_3$ in the infrared region, i.e., 12.39 μm, and reflectivity and transmission of $BaIrF_3$, exhibiting the metallic nature, requires the investigation of the complex dielectric function. Complex dielectric functions, which are typically used to explain how solids behave when electromagnetic waves (EMs) are present, can be exploited to learn more about how EM waves travel through different media and how electrons and phonons interact. The $\varepsilon_1(\omega)$, which is what accounts for the energy stored in any medium, can be used to extract the stored energy from the imaginary part of the dielectric function using Kramer−Kronig transformations.[44] Data on band topologies, absorption behavior, and charge carrier transitions from occupied to unoccupied levels are also provided by the $\varepsilon_2(\omega)$.[45−47] Figure 7a,b depicts the real and imaginary parts of the dielectric function for the materials under investigation. $\varepsilon(\omega)$ is utilized to determine the optical responses of the material. Because it represents the electronic aspect of the static dielectric constant and majorly depends on the band-gap value, the zero-frequency limit $\varepsilon_1(0)$ is an accurate measurement of $\varepsilon_1(\omega)$. Values of $\varepsilon_1(0)$ for $BaCoF_3$ and $BaIrF_3$ are 29.50 and 16.13, respectively.

https://doi.org/10.1021/acsomega.2c05845
ACS Omega 2023, 8, 5274−5284

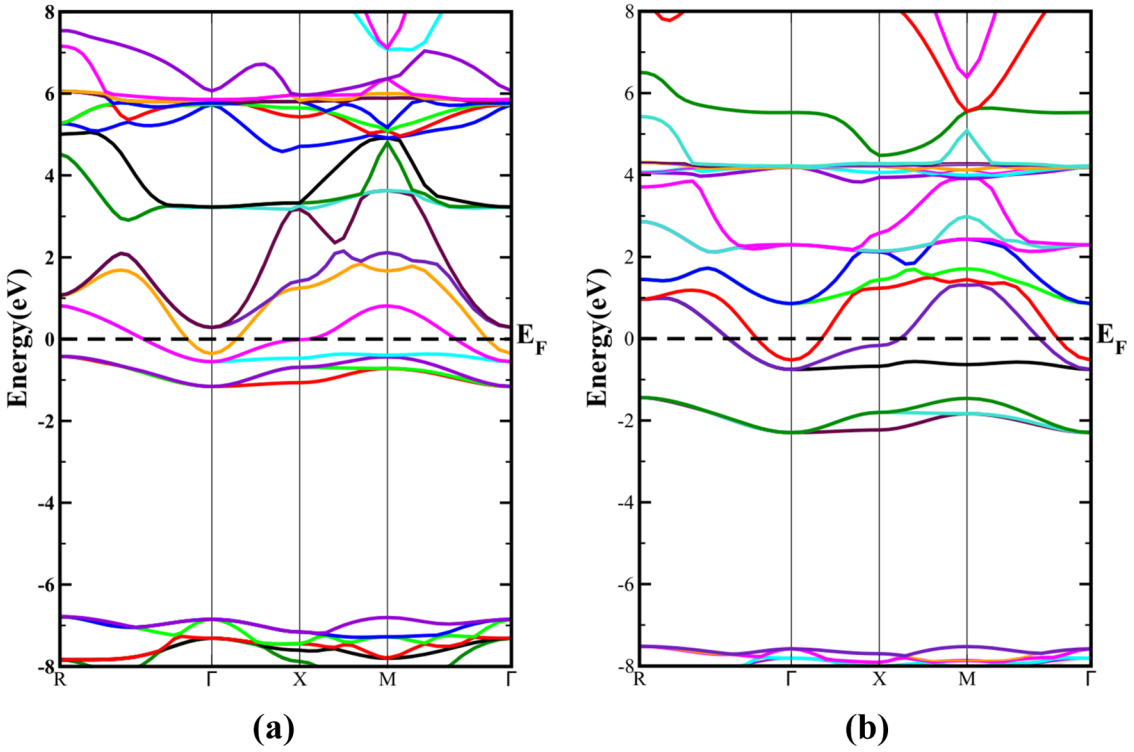

Figure 4. Band structure profile of the (a) $BaCoF_3$ and (b) $BaIrF_3$ fluoro-perovskites.

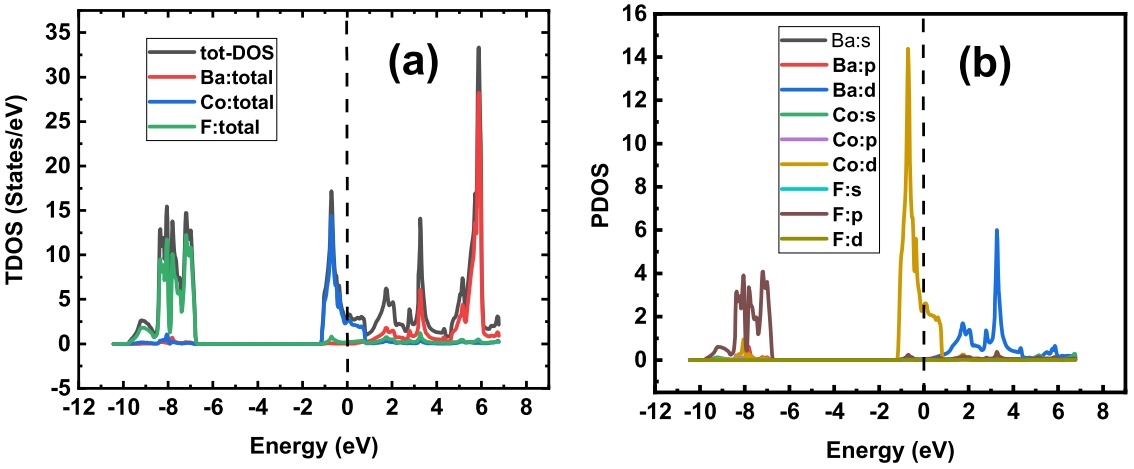

Figure 5. (a) Total density of states of the $BaCoF_3$ and (b) partial density of states.

The $\varepsilon_1(0)$ in the $BaCoF_3$ material reaches its maximum value at 0.01 eV, beyond which point it continues to degrade. On the other hand, the value of $\varepsilon_1(\omega)$ for $BaIrF_3$ falls after reaching a peak at 0.34 eV and moves into the negative zone. It is evident that $BaCoF_3$ is conducting for incident photons at all energy range, while $BaCoF_3$ turn out to be insulating for incident photons with higher energies [negative part of $\varepsilon_1(\omega)$]. Figure 7b shows how the stated compounds' imaginary portion of the dielectric constant behaves. It is well known that the biggest determinant of the electrical behavior of crystalline materials is the photon absorption-related quantity $\varepsilon_2(\omega)$ The initial peak in the $\varepsilon_2(\omega)$ spectra of $BaCoF_3$ and $BaIrF_3$ emerges at 0.01 and 0.55, respectively, according to Figure 7b, and thereafter decreases as energy increases. These peak locations mark the change from valance to CB. Since $BaCaF_3$ fluoro-perovskite has a direct band gap, its optical transition is also a direct band gap in nature. It is also abundantly obvious from the compounds' PDOS that these transitions are mostly caused by the Ba-p, Co-d, and F-p. Furthermore, as each researched compound has a distinct value for its dielectric function in various dimensions, its real and imaginary parts for the present materials reveal their anisotropy. When an electron moves quickly through a medium, energy is lost. This energy loss can cause several events, including phonon and plasmon excitation, interband transition, and inner shell ionization.[48] The plasma frequency is when the energy loss function reaches its highest value.[32] According to the energy loss spectra shown in Figure 7c, the static level for any of the compounds demonstrates no energy loss, but the energy loss peak for $BaCoF_3$ starts at 3.85 eV and for $BaIrF_3$ appears at 4.55 eV. The energy loss values start increasing dramatically at a higher energy range between 10 and 14 eV for both materials. The absorption coefficient is

https://doi.org/10.1021/acsomega.2c05845
ACS Omega 2023, 8, 5274−5284

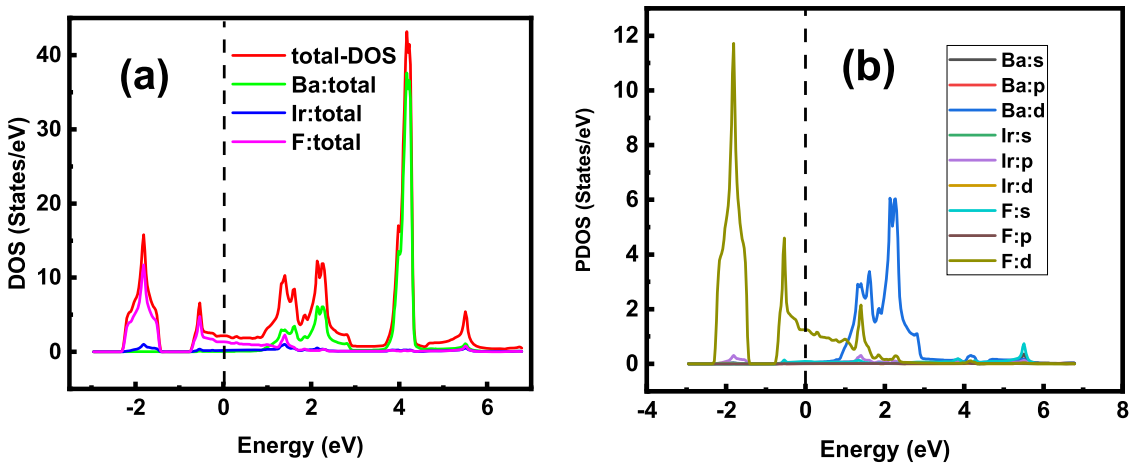

Figure 6. (a) Total density of states of the $BaIrF_3$ and (b) partial density of states.

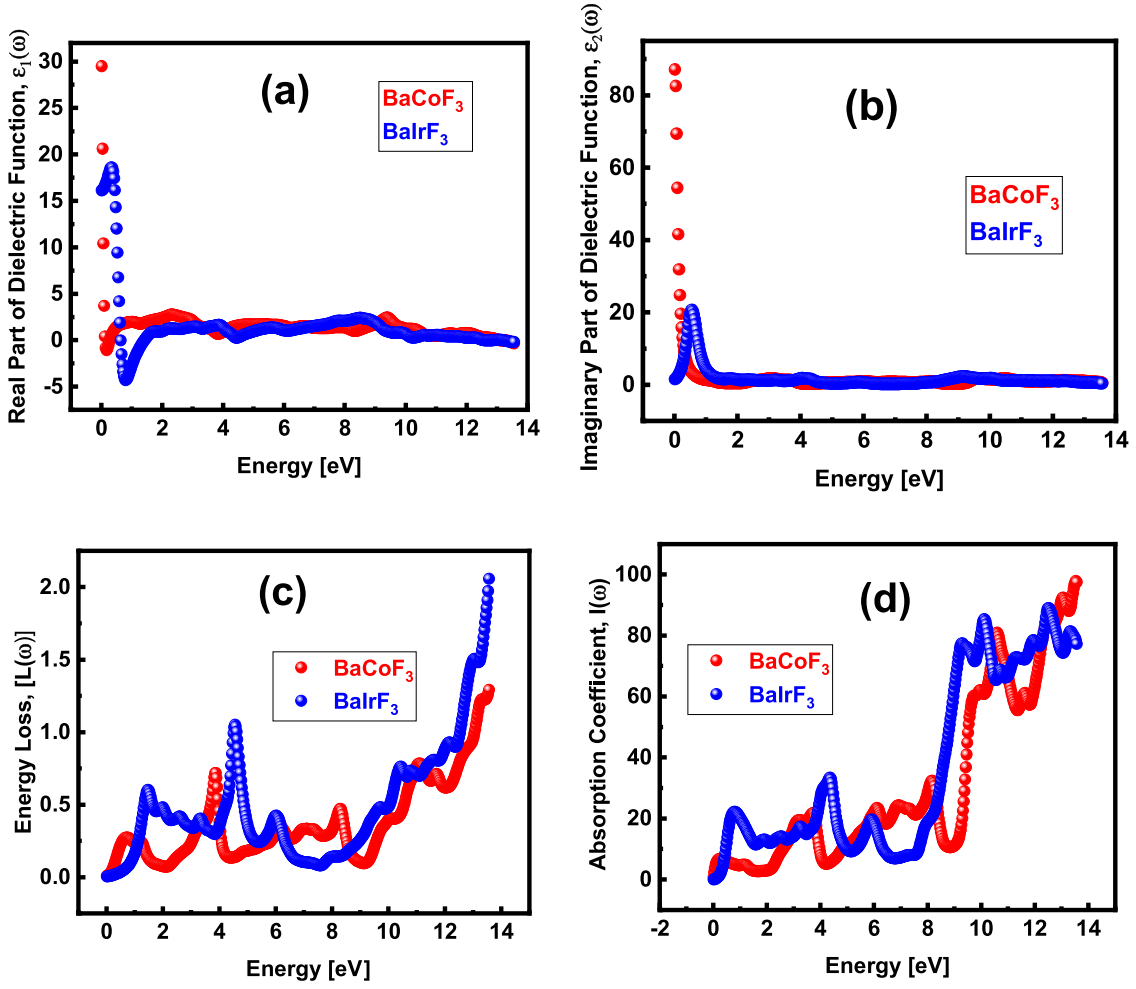

Figure 7. (a) Real and (b) imaginary parts of the dielectric function, (c) energy loss function, and (d) absorption coefficient for the $BaCoF_3$ (represented by red data points) and $BaIrF_3$ (represented by blue data points).

another significant parameter employed to measure light absorption. The attenuation of light intensity and distance as it travels through the material may be measured using its spectrum, and how it behaves can be anticipated by using the dielectric function. The energy absorption spectra [Figure 7d] for both materials show that there is no absorption peak in the infrared (IR) or visible energy range, indicating that the compounds demonstrate transparency in these regions. The absorption coefficient has maximum absorption $I(\omega)$ peaks in the UV region at 10.73 and 10.70 eV, respectively. For both materials, the UV region is where intense light absorption occurs. The generation of absorption peaks results from the electrons' interband transition. These materials present a

https://doi.org/10.1021/acsomega.2c05845
ACS Omega 2023, 8, 5274−5284

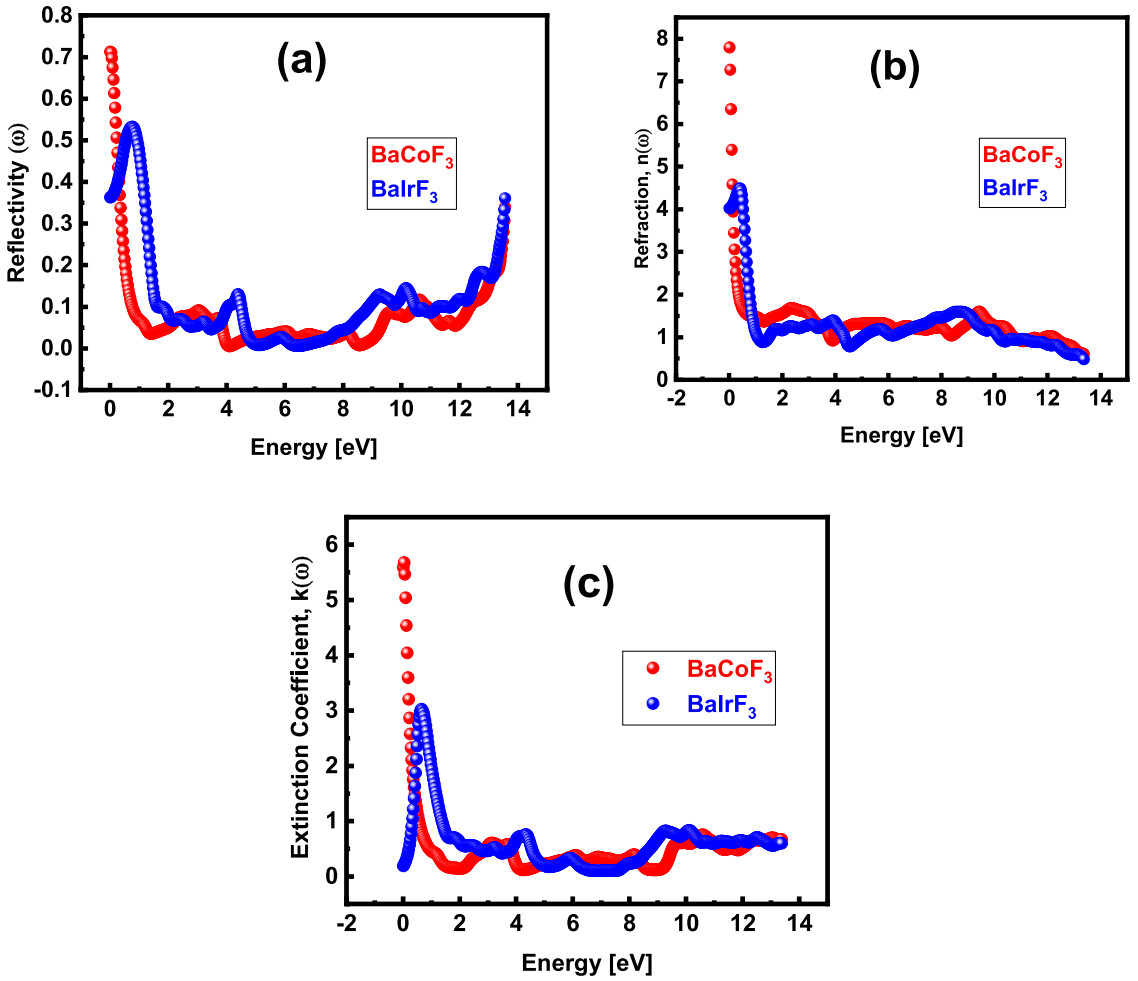

Figure 8. (a) Reflectivity, (b) refraction, and (c) extinction coefficient of the $BaCoF_3$ and $BaIrF_3$ fluoro-perovskites, represented by red and blue data points, respectively.

potential for optoelectronics applications as they do not absorb light in the visible spectrum.

Reflectivity, $R(\omega)$, is a crucial factor since it evaluates a substance's suitability for shielding application due to its antireflective coating. The reflectivity spectra of the materials under investigation are displayed in Figure 8a, where at the static level, $BaCoF_3$ and $BaIrF_3$ have $R(\omega)$ values of 0.72 and 0.35, respectively. After reaching a static level, reflectance drops abruptly for the $BaCoF_3$, while it continues to increase and reaches its maximum at about 0.70 eV. In the energy ranging from 0 to 14 eV, the determined refractive index for $BaCoF_3$ (red) and $BaIrF_3$ (blue) is 7.84 and 4.65, at a lower energy of 0.12 and 3.82 eV, respectively, as shown in Figure 8b. The curves for b materials coincide and begin to drop with increasing energy and flatten for the rest of the energy. The fact that $BaCoF_3$ has a greater refractive index than $BaIrF_3$ does suggest that the photons are more delayed because of electronic polarization while passing through the former's medium. The size of the atoms that make up the material determines the degree of electronic polarization: an Ir atom with a bigger size creates a stronger polarization, which causes higher retardation (slower velocity) of the photon inside the material and, consequently, a lower refractive index. For both materials, it falls to 0.50 at around 13.50 eV.

The extinction coefficient, $k(\omega)$, was derived to show how much light a material absorbs.

The extinction coefficients for $BaCoF_3$ and $BaIrF_3$, which are shown in Figure 8c as red- and blue-colored data, respectively, have maximum values of 5.70 and 3.12 at 0.15 and 0.56 eV, respectively. For both materials, the extinction coefficient drops dramatically and diminishes at higher energies while fluctuating slightly.

3.4. Thermoelectric Properties. The thermoelectricity of the compounds is investigated for energy conversion and their uses in thermoelectric refrigeration, computer cooling, and tiny detector components. The thermoelectric effect is brought about by the production of potential difference, which, in turn, results in the generation of the heat gradient. We measured the negative formation energies of −1.3 and −2.5 eV, respectively, for $BaCoF_3$ and $BaIrF_3$, confirming the thermodynamic stability of these materials. Thermal conductivity (κ/τ), Seebeck coefficient (S), specific heat capacity (C_v), and power factor (PF) for $BaCoF_3$ and $BaIrF_3$ vs temperature are studied in Figure 9a−d. The increased thermoelectric efficiency is supported by the low thermal conductivity, high electrical conductivity, and higher Seebeck value. The crucial element, the Seebeck coefficient, or thermopower, is given by the ratio of the voltage change to temperature change $(S = \Delta V/\Delta T)$. Subject to the type of charge, it may have a positive or negative value: the positive value indicates holes, while the negative value indicates electrons. Figure 9a shows how the predicted Seebeck coefficient changes with temperature for the

https://doi.org/10.1021/acsomega.2c05845
ACS Omega 2023, 8, 5274−5284

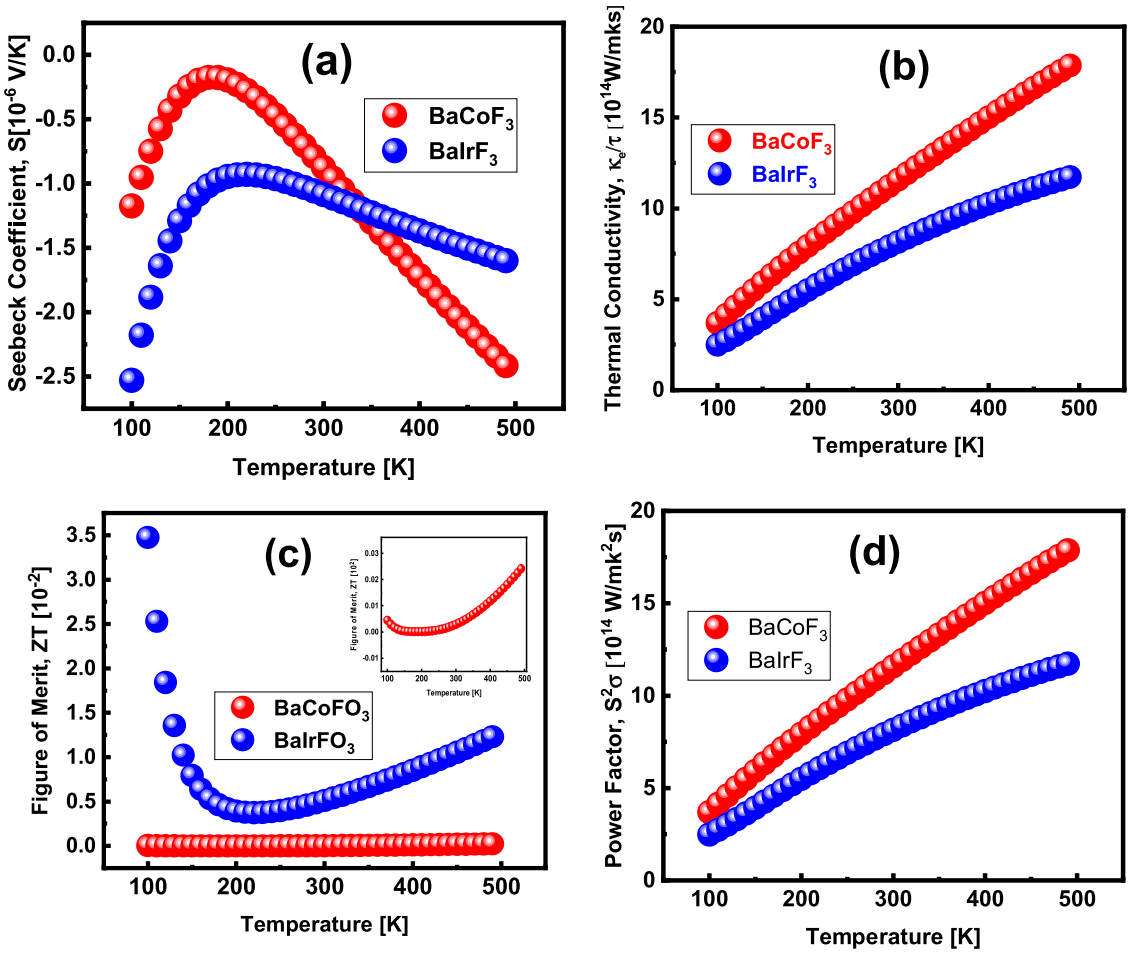

Figure 9. (a) Seebeck coefficient, (b) thermal conductivity, (c) figure of merit, and (d) power factor for the $BaCoF_3$ and $BaIrF_3$ fluoro-perovskites, represented by red and blue data points, respectively.

two materials $BaCoF_3$ and $BaIrF_3$, where the S starts to increase with the increase in temperature from 100 to 200 K, followed by a decrease in it with a further increase in the temperature from 200 to 500 K. The increase in S is attributed to a perfect concentration of the holes where the Seebeck coefficient begins to increase as the temperature increases. Since thermally stimulated electrons dominate the transport behavior, the decline in the Seebeck coefficient value is primarily attributed to this. At an ambient temperature, $BaCoF_3$ has a larger Seebeck coefficient value than $BaIrF_3$. In comparison to the $BaCoF_3$ curve, the $BaIrF_3$ curve is flatter due to a lower Seebeck coefficient and higher thermal conductivity. Figure 8a also shows that the Seebeck coefficient has negative values over the entire range of temperature, which shows that the dominant charge carriers are electrons. This suggests the n-type nature of the semiconductor. A crystal lattice's thermal conductivity (κ/τ) quantifies the thermal current generated by the combined electron and phonon energy. The materials with a κ/τ are frequently used in applications requiring heat sinks and low-value thermal insulation. Lattice vibrations, the source of mechanical elastic waves for phonon contributions and free carriers for electron contributions, are created because of the increase in temperature. The temperature-dependent κ/τ for both materials is shown in Figure 9b. Owing to the high electron energy, $BaCoF_3$ has a substantially steeper slope than $BaIrF_3$. Unlike the $BaIrF_3$, which has a maximum figure of merit (ZT) of 0.03 at a 100 K temperature and dramatically decreases with increasing temperature, $BaCoF_3$ has a smaller ZT value, and the value does not abruptly change [Figure 9c]. However, the inset of Figure 9c illustrates the curve of the ZT for the $BaCoF_3$. The power factor (PF), which is theoretically represented as PF = $\sigma S^2/t$, assesses thermoelectric efficiency without taking thermal conductivity into account in terms of the square of the Seebeck coefficient (S) and electrical conductivity (σ/τ). For both materials, the PF value reaches its maximum at 500 K, but the PF increase for $BaCoF_3$ is more than that for $BaIrF_3$.

The magnetic reaction of a material is described by its susceptibility. For $BaCoF_3$, the susceptibility increases from 1.56×10^{-11} to 1.74×10^{-11} m^3 mol^{-1} with increasing temperature from 100 to 250 K but gets saturated with a further increase in temperature [Figure 10a], which is attributed to heat effects on electron spin movement. On the other hand, for $BaIrF_3$ material, it decreases from 1.85×10^{-11} to 1.77×10^{-11} while increasing the temperature from 100 to 208 K. This decrease is explained based on thermal effects on electron spin movement. Both charge carriers and phonons are included in the specific heat capacity (C_v) of solids. To see the Dulong–Petit behavior, the C_v vs temperature is plotted in Figure 10b, where for $BaCoF_3$ it leads the one for $BaIrF_3$, with the increase in temperature ranging from 50 to 250 K and gets saturated with further increasing the temperature up to 950 K at around 124. The vibrational contribution in the C_v reaches around $3R$ at 50 K. Since both compounds exhibit a metallic

https://doi.org/10.1021/acsomega.2c05845
ACS Omega 2023, 8, 5274−5284

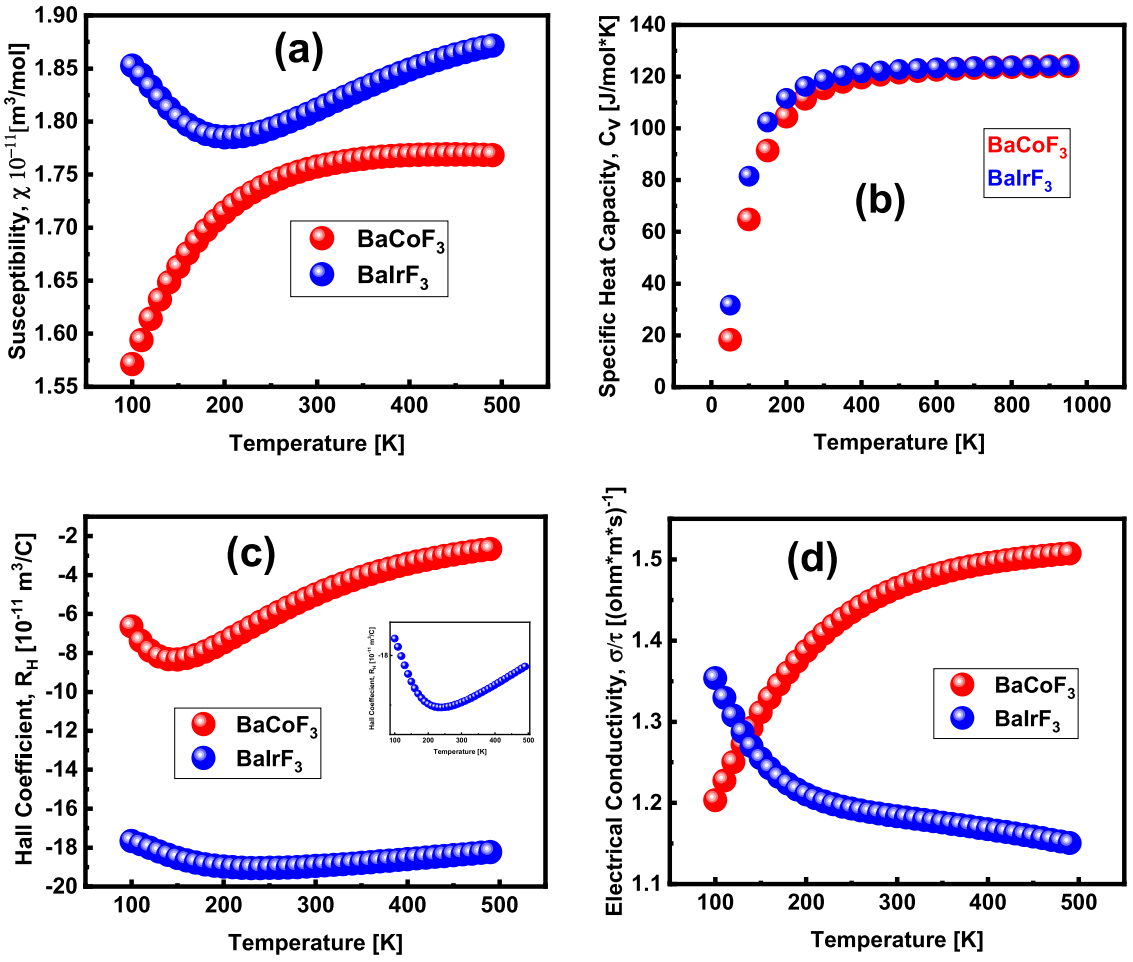

Figure 10. (a) Susceptibility, (b) specific heat capacity, (c) Hall coefficient, and (d) electrical conductivity for the $BaCoF_3$ and $BaIrF_3$ fluoro-perovskites, represented by red and blue data points, respectively.

nature, the phonon contribution dominates the electronic ones at high temperatures.

As demonstrated in the inset of Figure 10c, the Hall coefficient is high at low temperatures for $BaIrF_3$ and drops exponentially with increasing temperatures from 100 to 220 K as carriers become more conductive. However, it starts increasing with a further increase in temperature like in the case of $BaCoF_3$. A negative Hall coefficient was calculated for each of the two materials, indicating that they are both p-type conducting materials: in each of the examined materials, the holes dominate in electronic transport. Figure 10d shows that the electrical conductivity of $BaCoF_3$ elevates with the increase in temperature while gaining saturation at higher energies, whereas $BaIrF_3$ exhibits temperature-dependent decreases in conductivity. In the instance of $BaCoF_3$, the increase in electrical conductivity is most likely the result of a thermal disturbance between electrons and ions.

4. CONCLUSIONS

In conclusion, the structural and thermodynamical stability and optoelectronic and thermoelectric properties of $BaXF_3$ (X = Co, Ir) fluoro-perovskites were investigated while using the density functional theory coded within Wien2K. The structural stability of these fluoro-perovskites was confirmed by the Birch−Murnaghan fit to the energy-vs-volume data, while the thermodynamic stability was shown by the negative formation energy and phonon calculations for both compounds. The relation between elastic constants such as $C_{11} - C_{12} > 0$, $C_{11} > 0$, $C_{11} + 2C_{12} > 0$, and $B > 0$ revealed the mechanical stability of the compounds. With greater elastic stiffness coefficients, $BaIrF_3$ exhibited a strong ability to endure compressive and shear stresses. $BaCoF_3$ showed a weaker capacity of withstanding changes in volume due to a lower bulk modulus. Exhibiting a higher G-modulus of rigidity than the $BaIrF_3$, $BaCoF_3$ turned out to be stronger for resisting a changing shape. Both compounds demonstrated anisotropy and brittleness. The band gaps revealed the metallic nature of the $BaCoF_3$ and $BaIrF_3$. Furthermore, the metallic nature of $BaCoF_3$ and $BaIrF_3$ was also validated by the density-of-states study, where Co and F atoms contributed significantly to the TDOS in the valence band in the case of $BaCoF_3$, while the TDOS of $BaIrF_3$ was dominated by the Ba and F atoms. The computed values of $\varepsilon_1(0)$ for $BaCoF_3$ and $BaIrF_3$ are approximately 30 and 19, respectively, which were in line with Penn's model. The researched materials were confirmed to be strong contenders for optoelectronics by the lack of absorption in the visible range. For their potential use in thermoelectric device applications, the Seebeck coefficient, specific heat capacity, thermal conductivity, power factor (PF), and figure of merit as a function of temperature were also investigated, which showed that these materials are thermally stable and preset potentiality to be used in thermoelectric devices.

https://doi.org/10.1021/acsomega.2c05845
ACS Omega 2023, 8, 5274−5284

AUTHOR INFORMATION

Corresponding Author

Shaukat Ali Khattak − *Department of Physics, Abdul Wali Khan University, 23200 Mardan, Pakistan;* orcid.org/0000-0003-3471-6237; Email: shaukat.khattak@awkum.edu.pk

Authors

Mohammed Abohashrh − *Department of Basic Medical Sciences, College of Applied Medical Sciences, King Khalid University, Abha 61421, Kingdom of Saudi Arabia*

Imtiaz Ahmad − *Department of Chemistry, Fatima Jinnah Women University, 46000 Rawalpindi, Pakistan;* orcid.org/0000-0003-1599-6181

Mudasser Husain − *Department of Physics, University of Lakki Marwat, 28420 Lakki Marwat, Pakistan*

Irfan Ullah − *Department of Physics, Abdul Wali Khan University, 23200 Mardan, Pakistan*

Syed Zulfiqar − *Department of Physics, Abdul Wali Khan University, 23200 Mardan, Pakistan*

Gul Rooh − *Department of Physics, Abdul Wali Khan University, 23200 Mardan, Pakistan*

Nasir Rahman − *Department of Physics, University of Lakki Marwat, 28420 Lakki Marwat, Pakistan*

Gulzar Khan − *Department of Physics, Abdul Wali Khan University, 23200 Mardan, Pakistan*

Tahirzeb Khan − *Department of Physics, Abdul Wali Khan University, 23200 Mardan, Pakistan*

Muhammad Salman Khan − *Department of Physics, Abdul Wali Khan University, 23200 Mardan, Pakistan;* orcid.org/0000-0001-9909-0883

Said Karim Shah − *Department of Physics, Abdul Wali Khan University, 23200 Mardan, Pakistan;* orcid.org/0000-0003-0942-2464

Vineet Tirth − *Mechanical Engineering Department, College of Engineering, King Khalid University, Abha 61421, Kingdom of Saudi Arabia; Research Center for Advanced Materials Science (RCAMS), King Khalid University, Guraiger, Abha 61413 Asir, Kingdom of Saudi Arabia*

Complete contact information is available at: https://pubs.acs.org/10.1021/acsomega.2c05845

Notes

The authors declare no competing financial interest.

ACKNOWLEDGMENTS

The authors extend their appreciation to the Deanship of Scientific Research at King Khalid University for funding this work through the Small Groups Project under grant number RGP.1/368/43. The authors would like to thank the National Research Program for Universities (NRPU), Higher Education Commission Pakistan, No. 20-8862/NRPU/R&D/HEC/2017, the National Research Program for Universities (NRPU), Higher Education Commission Pakistan, No. 20-15131/NRPU/R&D/HEC/2021, and the National Research Program for Universities (NRPU), Higher Education Commission Pakistan, No. 20-15128/NRPU/R&D/HEC/2021.

REFERENCES

(1) Nishimatsu, T.; Terakubo, N.; Mizuseki, H.; Kawazoe, Y.; Pawlak, D. A.; Shimamura, K.; Fukuda, T. Band Structures of Perovskite-like Fluorides for Vacuum-Ultraviolet-Transparent Lens Materials. *Jpn. J. Appl. Phys.* **2002**, *41*, No. L365.

(2) Vanderbilt, D. Soft Self-Consistent Pseudopotentials in a Generalized Eigenvalue Formalism. *Phys. Rev. B* **1990**, *41*, No. 7892.

(3) Ouenzerfi, R. El.; Ono, S.; Quema, A.; Goto, M.; Sarukura, N.; Nishimatsu, T.; Terakubo, N.; Mizuseki, H.; Kawazoe, Y.; Yoshikawa, A.; Fukuda, T. Design Proposal of Light Emitting Diode in Vacuum Ultraviolet Based on Perovskite-like Fluoride Crystals. *Jpn. J. Appl. Phys.* **2004**, *43*, No. L1140.

(4) Guo, S. D.; Liu, B. G. Electronic Structures and Optical Dielectric Functions of Room Temperature Phases of $SrTiO_3$ and BaTiO3. *J. Appl. Phys.* **2011**, *110*, No. 073525.

(5) Khan, W.; Borek, S.; Minar, J. Correlation between the Electronic Structure, Effective Mass and Thermoelectric Properties of Rare Earth Tellurides Ba_2MYTe_5 (M = Ga, In). *RSC Adv.* **2015**, *5*, 51461−51469.

(6) Šipr, O.; Khan, W.; Joly, Y.; Minár, J. Ca and S K-Edge XANES of CaS Calculated by Different Methods: Influence of Full Potential, Core Hole and Eu Doping. *J. Synchrotron Radiat.* **2019**, *26*, 152−158.

(7) Murtaza, G.; Ahmad, I.; Afaq, A. Shift of Indirect to Direct Bandgap in Going from K to Cs in $MCaF_3$ (M = K, Rb, Cs). *Solid State Sci.* **2013**, *16*, 152−157.

(8) Singh, N.; Saini, S. M.; Nautiyal, T.; Auluck, S. Electronic Structure and Optical Properties of Rare Earth Sesquioxides (R_2O_3, R=La, Pr, and Nd. *J. Appl. Phys.* **2006**, *100*, No. 083525.

(9) Saini, S. M.; Singh, N.; Nautiyal, T.; Auluck, S. Comparative Study of Optical and Magneto-Optical Properties of $GdFe_2$ and $GdCo_2$. *J. Phys.: Condens. Matter* **2007**, *19*, No. 176203.

(10) Singh, N.; Schwingenschlögl, U. High Eu 4f Low-Energy Oscillator Strength in the Isostructural Rare-Earth Zintl Compounds $EuIn_2X_2$ (X = P,As). *Appl. Phys. Lett.* **2012**, *100*, No. 151906.

(11) Singh, N.; Mohan Saini, S.; Nautiyal, T.; Auluck, S. Theoretical Investigation of the Optical and Magneto-Optical Properties of EuX (X=S, Se, and Te). *Phys. B* **2007**, *388*, 99−106.

(12) Murtaza, G.; Hayatullah; Khenata, R.; Khalid, M. N.; Naeem, S. Elastic and Optoelectronic Properties of $RbMF_3$ (M=Zn, Cd, Hg): A MBJ Density Functional Calculation. *Phys. B* **2013**, *410*, 131−136.

(13) Ono, S.; El Ouenzerfi, R.; Quema, A.; Murakami, H.; Sarukura, N.; Nishimatsu, T.; Terakubo, N.; Mizuseki, H.; Kawazoe, Y.; Yoshikawa, A.; Fukuda, T. Band-Structure Design of Fluoride Complex Materials for Deep-Ultraviolet Light-Emitting Diodes. *Jpn. J. Appl. Phys.* **2005**, *44*, 7285−7290.

(14) Studzinski, P.; Spaeth1, J. M. ENDOR Investigation of the Structural Phase Transition in $RbCdF_3$. *J. Phys. C Solid State Phys.* **1986**, *19*, No. 6441.

(15) Chornodolskyy, Y.; Syrotyuk, S.; Stryganyuk, G.; Voloshinovskii, A.; Rodnyi, P. Electronic Energy Structure and Core-Valence Luminescence of ABX_3 (A = K, Rb, Cs; B = Ca; X = F) Crystals. *J. Phys. Stud.* **2007**, *11*, 421−426.

(16) Babu, K. E.; Veeraiah, A.; Swamy, D. T.; Veeraiah, V. First-Principles Study of Electronic Structure and Optical Properties of Cubic Perovskite $CsCaF_3$. *Chin. Phys. Lett.* **2012**, *29*, No. 117102.

(17) Mousa, A. A.; Khalifa, J. M.; M, N. T. First Principles Study of Structural, Electronic and Optical Properties of the Fluoroperovskite $RbCaF_3$ Crystal. *Am. J. Condens. Matter Phys.* **2013**, *3*, 151−162.

(18) Li, Z.-L.; An, X.-Y.; Cheng, X.-L.; Wang, X.-M.; Zhang, H.; Peng, L.-P.; Wu, W.-D. First-Principles Study of the Electronic Structure and Optical Properties of Cubic Perovskite $NaMgF_3$. *Chin. Phys. B* **2014**, *23*, No. 037104.

(19) Bulou, A.; Ridou, C.; Rousseau, M.; Nouet, J.; Hewat, A. The Temperature Dependence of the Structures of $RbCaF_3$, and the Determination of the Low Temperature Phases. *J. Phys.* **1980**, *41*, 87−96.

(20) Tran, F.; Blaha, P. Accurate Band Gaps of Semiconductors and Insulators with a Semilocal Exchange-Correlation Potential. *Phys. Rev. Lett.* **2009**, *102*, No. 226401.

(21) Natarajan, M.; Prakash, B. Phase Transitions in ABX_3 Type Halides. *Phys. Status Solidi A* **1971**, *4*, K167−K172.

(22) Kohn, W.; Sham, L. J. Self-Consistent Equations Including Exchange and Correlation Effects. *Phys. Rev.* **1965**, *140*, No. A1133.

(23) Blaha, P.; Schwarz, K.; Madsen, G. K. H.; Kvasnicka, D.; Luitz, J.; Laskowsk, R.; Tran, F.; Marks, L.; Marks, L. WIEN2k: An Augmented Plane Wave Plus Local Orbitals Program for Calculating Crystal Properties. *Uniw. śląski* **2019**, 343−354.
(24) Mun Wong, K.; Alay-E-Abbas, S. M.; Shaukat, A.; Fang, Y.; Lei, Y. First-Principles Investigation of the Size-Dependent Structural Stability and Electronic Properties of O-Vacancies at the ZnO Polar and Non-Polar Surfaces. *J. Appl. Phys.* **2013**, *113*, No. 014304.
(25) Mun Wong, K.; Alay-E-Abbas, S. M.; Fang, Y.; Shaukat, A.; Lei, Y. Spatial Distribution of Neutral Oxygen Vacancies on ZnO Nanowire Surfaces: An Investigation Combining Confocal Microscopy and First Principles Calculations. *J. Appl. Phys.* **2013**, *114*, No. 034901.
(26) Khan, W.; Murtaza, G.; Ouahrani, T.; Mahmood, A.; Khenata, R.; El Amine Monir, M.; Baltache, H. Electronic, Bonding, Linear and Non-Linear Optical Properties of Novel $Li_2Ga_2GeS_6$ Compound. *J. Alloys Compd.* **2016**, *674*, 109−115.
(27) Khan, A. A.; Khan, W.; Khan, A.; Laref, A.; Zeb, A.; Murtaza, G. Investigation of the Structural, Electrical, Optical and Magnetic Properties of $XMg_4Mn_6O_{15}$ (X = K, Rb, and Cs) Compounds. *Mater. Res. Express* **2019**, *6*, No. 066102.
(28) Sandeep; Rai, D. P.; Shankar, A.; Ghimire, M. P.; Khenata, R.; Bin Omran, S.; Syrotyuk, S. V.; Thapa, R. K. Investigation of the Structural, Electronic and Optical Properties of the Cubic $RbMF_3$ Perovskites (M = Be, Mg, Ca, Sr and Ba) Using Modified Becke-Johnson Exchange Potential. *Mater. Chem. Phys.* **2017**, *192*, 282−290.
(29) Yousaf, M.; Saeed, M. A.; Ahmed, R.; Alsardia, M. M.; Isa, A. R. M.; Shaari, A. An Improved Study of Electronic Band Structure and Optical Parameters of X-Phosphides (X=B, Al, Ga, In) by Modified Becke—Johnson Potential. *Commun. Theor. Phys.* **2012**, *58*, No. 777.
(30) Krasovskii, E. E.; Schattke, W. Local Field Effects in Optical Excitations of Semicore Electrons. *Phys. Rev. B* **1999**, *60*, No. R16251.
(31) Krasovska, O. V.; Antonov, V. N.; Krasovskii, E. E.; Schattke, W. Effect of Off-Diagonal Dielectric Response on Optical Properties of $LaTiO_3$. *Phys. Status Solidi B* **2006**, *243*, 1885−1892.
(32) Khan, M. S.; Gul, B.; Khan, G.; Benaadad, M.; Ghlamallah, B.; Khattak, S. A.; Khan, T.; Zulfiqar, S.; Shah, S. K.; Khan, M. A. Ab-Initio Study about the Electronic, Optical and Thermoelectric Nature of α-, β-, and γ-Phases of CdS Semiconductor: Using the Accurate m-BJ Approach. *Phys. Scr.* **2021**, *96*, No. 055803.
(33) Katsura, T.; Tange, Y. A Simple Derivation of the Birch−Murnaghan Equations of State (EOSs) and Comparison with EOSs Derived from Other Definitions of Finite Strain. *Minerals* **2019**, *9*, No. 745.
(34) Ravindran, P.; Fast, L.; Korzhavyi, P. A.; Johansson, B.; Wills, J.; Eriksson, O. Density Functional Theory for Calculation of Elastic Properties of Orthorhombic Crystals: Application to $TiSi_2$. *J. Appl. Phys.* **1998**, *84*, No. 4891.
(35) Bockstedte, M.; Kley, A.; Neugebauer, J.; Scheffler, M. Density-Functional Theory Calculations for Poly-Atomic Systems: Electronic Structure, Static and Elastic Properties and Ab Initio Molecular Dynamics. *Comput. Phys. Commun.* **1997**, *107*, 187−222.
(36) Luo, X.; Wang, B. Structural and Elastic Properties of $LaAlO_3$ from First-Principles Calculations. *J. Appl. Phys.* **2008**, *104*, No. 073518.
(37) Solid State Physics: Ashcroft, Neil W., Mermin, N. David + Free Shipping, 2022. https://www.amazon.com/Solid-State-Physics-Neil-Ashcroft/dp/0030839939 (accessed Nov 16, 2022).
(38) Khattak, S. A.; Wabaidur, S. M.; Islam, M. A.; Husain, M.; Ullah, I.; Zulfiqar, S.; Rooh, G.; Rahman, N.; Khan, M. S.; Khan, G.; Khan, T. First-Principles Structural, Elastic and Optoelectronics Study of Sodium Niobate and Tantalate Perovskites. *Sci. Rep.* **2022**, *12*, No. 21700.
(39) Khan, H.; Sohail, M.; Rahman, N.; Hussain, M.; Khan, A.; Hegazy, H. H. Theoretical Study of Different Aspects of Al-Based Fluoroperovskite AlMF (M = Cu, Mn) Compounds Using TB-MBJ Potential Approximation Method for Generation of Energy. *Results Phys.* **2022**, *42*, No. 105982.
(40) Vaitheeswaran, G.; Kanchana, V.; Kumar, R. S.; Cornelius, A. L.; Nicol, M. F.; Svane, A.; Delin, A.; Johansson, B. High-Pressure Structural, Elastic, and Electronic Properties of the Scintillator Host Material $KMgF_3$. *Phys. Rev. B* **2007**, *76*, No. 014107.
(41) Yang, B.; Wang, L.; Han, J.; Zhou, Y.; Song, H.; Chen, S.; Zhong, J.; Lv, L.; Niu, D.; Tang, J. $CuSbS_2$ as a Promising Earth-Abundant Photovoltaic Absorber Material: A Combined Theoretical and Experimental Study. *Chem. Mater.* **2014**, *26*, 3135−3143.
(42) Azam, S.; Kamran, M. A.; Iqbal, M. W.; Irfan, M.; Qaiser, T.; Salman Khan, M.; Alharbi, T.; Majid, A.; Khenata, R.; Omran, S.; Bin; Wang, X. Ab-Initio Study of Cu-Based Oxychalcogenides: A New Class of Materials for Optoelectronic Applications. *J. Solid State Chem.* **2020**, *284*, No. 121191.
(43) Dai, C. M.; Xu, P.; Huang, M.; Cai, Z. H.; Han, D.; Wu, Y.; Chen, S. $NaSbSe_2$ as a Promising Light-Absorber Semiconductor in Solar Cells: First-Principles Insights. *APL Mater.* **2019**, *7*, No. 081122.
(44) Khan, M. S.; Alshahrani, T.; Haq, B. U.; Azam, S.; Khan, G.; Alrobei, H.; Abbas, Z.; Předota, M.; Khan, M. A.; Benaadad, M. Investigation of Structural, Electronic and Optical Properties of Potassium and Lithium Based Ternary Selenoindate: Using First Principles Approach. *J. Solid State Chem.* **2021**, *293*, No. 121778.
(45) Rano, B. R.; Syed, I. M.; Naqib, S. H. Ab Initio Approach to the Elastic, Electronic, and Optical Properties of $MoTe_2$ Topological Weyl Semimetal. *J. Alloys Compd.* **2020**, *829*, No. 154522.
(46) Wang, D.; Tang, K.; Liang, Z.; Zheng, H. Synthesis, Crystal Structure, and Photocatalytic Activity of the New Three-Layer Aurivillius Phases, $Bi_2ASrTi_2TaO_{12}$ (A = Bi, La. *J. Solid State Chem.* **2010**, *183*, 361−366.
(47) Reshak, A. H.; Piasecki, M.; Auluck, S.; Kityk, I. V.; Khenata, R.; Andriyevsky, B.; Cobet, C.; Esser, N.; Majchrowski, A.; Świrkowicz, M.; Diduszko, R.; Szyrski, W. Effect of U on the Electronic Properties of Neodymium Gállate ($NdGaO_3$): Theoretical and Experimental Studies. *J. Phys. Chem. B* **2009**, *113*, 15237−15242.
(48) Ouahrani, T.; Otero-De-La-Roza, A.; Reshak, A. H.; Khenata, R.; Faraoun, H. I.; Amrani, B.; Mebrouki, M.; Luaa, V. Elastic Properties and Bonding of the $AgGaSe_2$ Chalcopyrite. *Phys. B: Condens. Matter* **2010**, *405*, 3658−3664.

https://doi.org/10.1021/acsomega.2c05845
ACS Omega 2023, 8, 5274−5284